

On the sensitivity of the HAWC observatory to gamma-ray bursts

A. U. Abeysekara^a, J. A. Aguilar^b, S. Aguilar^c, R. Alfaro^c, E. Almaraz^c, C. Álvarez^d,
 J. de D. Álvarez-Romero^e, M. Álvarez^c, R. Arceo^d, J. C. Arteaga-Velázquez^e, C. Badillo^c, A. Barber^f,
 B. M. Baughman^g, N. Bautista-Elivar^h, E. Belmont^c, E. Benítezⁱ, S. Y. BenZvi^b, D. Berley^g, A. Bernal^l,
 E. Bonamente^j, J. Braun^g, R. Caballero-Lopez^k, I. Cabrera^c, A. Carramiñana^l, L. Carrasco^l, M. Castillo^m,
 L. Chambersⁿ, R. Conde^m, P. Condreayⁿ, U. Cotti^e, J. Cotzomi^m, J. C. D'Olivo^o, E. de la Fuente^p, C. De
 León^e, S. Delay^q, D. Delepine^r, T. DeYoungⁿ, L. Diaz^o, L. Diaz-Cruz^m, B. L. Dingus^s, M. A. Duvernois^b,
 D. Edmunds^a, R. W. Ellsworth^t, B. Fick^j, D. W. Fiorino^b, A. Flandes^k, N. I. Fraijaⁱ, A. Galindo^l,
 J. L. García-Luna^p, G. García-Torales^p, F. Garfiasⁱ, L. X. González^l, M. M. Gonzálezⁱ, J. A. Goodman^g,
 V. Grabski^c, M. Gussert^u, C. Guzmán-Ceronⁱ, Z. Hampel-Arias^b, T. Harris^v, E. Hays^w,
 L. Hernandez-Cervantesⁱ, P. H. Hüntemeyer^j, A. Imran^s, A. Iriarteⁱ, J. J. Jimenez^d, P. Karn^q,
 N. Kelley-Hoskins^j, D. Kieda^f, R. Langaricaⁱ, A. Lara^k, R. Lauer^x, W. H. Leeⁱ, E. C. Linares^e,
 J. T. Linnemann^a, M. Longo^u, R. Luna-García^y, H. Martínez^z, J. Martínez^c, L. A. Martínezⁱ,
 O. Martínez^m, J. Martínez-Castro^y, M. Martosⁱ, J. Matthews^x, J. E. McEnery^w, G. Medina-Tanco^o,
 J. E. Mendoza-Torres^l, P. A. Miranda-Romagnoli^{aa}, T. Montaruli^b, E. Moreno^m, M. Mostafa^u,
 M. Napsuciale^r, J. Nava^l, L. Nellen^o, M. Newbold^f, R. Noriega-Papaqui^{aa}, T. Oceguera-Becerra^p,
 A. Olmos Tapia^l, V. Orozco^c, V. Pérez^c, E. G. Pérez-Pérez^h, J. S. Perkins^w, J. Pretz^s, C. Ramirez^m,
 I. Ramírez^c, D. Rebello^v, A. Rentería^c, J. Reyes^l, D. Rosa-González^l, A. Rosado^m, J. M. Ryan^{ab},
 J. R. Sacahuiⁱ, H. Salazar^m, F. Salesa^u, A. Sandoval^c, E. Santos^d, M. Schneider^{ac}, A. Shoup^{ad}, S. Silich^l,
 G. Sinnis^s, A. J. Smith^g, K. Sparksⁿ, W. Springer^f, F. Suárez^c, N. Suarez^l, I. Taboada^{v,*}, A. F. Tellez^m,
 G. Tenorio-Tagle^l, A. Tepe^v, P. A. Toale^{ae}, K. Tollefson^a, I. Torres^l, T. N. Ukwatta^a, J. Valdes-Galicia^k,
 P. Vanegas^c, V. Vasileiou^w, O. Vázquez^c, X. Vázquez^c, L. Villaseñor^e, W. Wall^l, J. S. Walters^l,
 D. Warner^u, S. Westerhoff^b, I. G. Wisher^b, J. Wood^g, G. B. Yodh^q, D. Zaborovⁿ, A. Zepeda^z

^aDepartment of Physics & Astronomy, Michigan State University, 3245 BPS Building, East Lansing, MI 48824, USA

^bDept. of Physics, University of Wisconsin - Madison, 1150 University Ave, WI 53706, USA

^cInstituto de Física, Universidad Nacional Autónoma de México, Apartado Postal 20-364, 01000 México D.F., México

^dCEFYMAP, Universidad Autónoma de Chiapas, 4a. Oriente Norte No. 1428, Col. La pimienta, Tuxtla Gutiérrez, Chiapas, 29040 México

^eUniversidad Michocana de San Nicolás de Hidalgo, Morelia, Mich. 58040, México

^fDepartment of Physics and Astronomy, University of Utah, Salt Lake City, UT 84112, USA

^gDept. of Physics, University of Maryland, College Park, MD 20742, USA

^hUniversidad Politécnica de Pachuca, Pachuca, Hidalgo, México

ⁱInstituto de Astronomía, Universidad Nacional Autónoma de México, México, D. F., 04510, México

^jDepartment of Physics, Michigan Technological University, Houghton, MI 49931, USA

^kInstituto de Geofísica, Universidad Nacional Autónoma de México, C.U. México D.F. 04510, México

^lInstituto Nacional de Astrofísica, Óptica y Electrónica, Luis Enrique Erro 1, Tonantzintla, Puebla 72840, México

^mFCFM, Benemérita Universidad Autónoma de Puebla, A.P. 1152, 72000 Puebla, México

ⁿDepartment of Physics, Pennsylvania State University, 104 Davey Laboratory, University Park, PA 16802, USA

^oInstituto de Ciencias Nucleares, Universidad Nacional Autónoma de México, México, D. F., 04510, México

^pCUCEI, CU-VALLES, CUCEA, Universidad de Guadalajara, Blvd. Marcelino García Barragán 1451, colonia Olímpica, 44430 Guadalajara, Jalisco, México

^qDepartment of Physics and Astronomy, University of California, Irvine, CA 92697, USA

^rDept. of Physics, Campus Leon, University of Guanajuato, Loma del Bosque 103, col. Loma del Campestre CP-37150 Leon, México

^sPhysics Division, Los Alamos National Laboratory, Los Alamos, NM 87545, USA

^tDepartment of Physics and Astronomy, George Mason University, Fairfax VA 22030, USA

^uColorado State University, 1875 Campus Delivery, Fort Collins, CO 80525, USA

^vSchool of Physics and Center for Relativistic Astrophysics, Georgia Institute of Technology, Atlanta, GA 30332, USA

^wNASA Goddard Space Flight Center, Greenbelt, MD 20771, USA

^xDepartment of Physics and Astronomy, University of New Mexico, Albuquerque, NM 87131, USA

^yCentro de Investigación en Computación, Instituto Politécnico Nacional, Av. J. de D. Bátiz, Esq. M. Othón de M. Col. Nva. Ind. Vallejo Del. G. A. M. CP 07738 México D.F., México

^zDepartment of Physics, Centro de Investigación y de Estudios Avanzados del IPN. P.O. Box 14-740, CP 07000, México DF, México

^{aa}Universidad Autónoma del Estado de Hidalgo. Pachuca, Hidalgo, México

^{ab}Department of Physics, University of New Hampshire, Morse Hall, Durham, NH 03824, USA

Abstract

We present the sensitivity of HAWC to Gamma Ray Bursts (GRBs). HAWC is a very high-energy gamma-ray observatory currently under construction in Mexico at an altitude of 4100 m. It will observe atmospheric air showers via the water Cherenkov method. HAWC will consist of 300 large water tanks instrumented with 4 photomultipliers each. HAWC has two data acquisition (DAQ) systems. The main DAQ system reads out coincident signals in the tanks and reconstructs the direction and energy of individual atmospheric showers. The scaler DAQ counts the hits in each photomultiplier tube (PMT) in the detector and searches for a statistical excess over the noise of all PMTs. We show that HAWC has a realistic opportunity to observe the high-energy power law components of GRBs that extend at least up to 30 GeV, as it has been observed by Fermi LAT. The two DAQ systems have an energy threshold that is low enough to observe events similar to GRB 090510 and GRB 090902b with the characteristics observed by Fermi LAT. HAWC will provide information about the high-energy spectra of GRBs which in turn could help to understanding about e-pair attenuation in GRB jets, extragalactic background light absorption, as well as establishing the highest energy to which GRBs accelerate particles.

Keywords: gamma-ray bursts, gamma ray

1. Introduction

Gamma-ray bursts (GRBs) are among the most powerful events in the universe [1, 2]. Suggested progenitors for GRBs include neutron star-neutron star or neutron star-black hole mergers [3, 4], millisecond proto-magnetars [5] and the core collapse of massive stars [6, 7]. Most of these theories have in common that the initial source for the energy output of the GRB is a central black hole surrounded by the remnant matter of the progenitor. A jetted, highly relativistic fireball interacting with itself or the surrounding interstellar matter, forming internal and external shocks in which Fermi-acceleration takes place, delivers a plausible explanation of the non-thermal spectrum of GRBs [8, 9, 10]. The boosted emission from GRBs explains why high-energy gamma rays are not attenuated via e-pair production [11]. However, the connection between accretion and jet production is poorly understood. The high luminosity of these events allows for their detection at very high redshifts [12], making them valuable for answering many astrophysical questions, even if their origin remains unclear. In particular, GRBs probe the content of the intervening space between their origin and Earth.

Measurements of gamma-ray light curves reveal two classes of bursts [13]: long and short GRBs, if they are longer or shorter than 2 s respectively. The prompt emission of a gamma-ray burst is typically described by the *Band function* [14]. The Band function is a good fit to the majority of GRB prompt spectra. Compton Gamma Ray Observatory (CGRO) data of GRB 941017 [15] and RHESSI data of GRB 021206 [16] showed that an additional hard power law component is sometimes present. As of mid-2011, the Fermi Large Area Telescope (Fermi LAT, which nominally operates between 30 MeV and 300 GeV) had detected 26 GRBs. Among these, the long GRB 090902b [17] and the short GRB 090510 [18] are notable for being very bright and having non-Band hard power-law components. To date, the highest energy photon recorded from a GRB is 33 GeV from GRB 090902b (or 94 GeV corrected for redshift) [17]. Fermi LAT probably did not detect higher energy gamma rays from GRB 090902b because of its limited size. Fermi Gamma-ray Burst

*Corresponding author: ignacio.taboada@physics.gatech.edu

Monitor (Fermi-GBM, which operates between 8 keV and 40 MeV), provided observations of the short bursts GRB 090227B and GRB 090228 [19] that are also best explained by including an additional hard non-Band component. Milagrito, predecessor of the Milagro detector, reported a possible detection of gamma rays in the TeV energy range from GRB 970417A at 3σ level [20]. Additional searches by Milagro over 7 years, did not result in significant observations [21, 22, 23]. The non-Band component is currently a challenge to GRB models. Among others, it has been interpreted as proton synchrotron radiation in the prompt phase [24] or electron synchrotron radiation in the early afterglow phase [25].

An observed GRB high-energy spectral cutoff can provide information about the source itself and the propagation of the gamma rays through the interstellar media (ISM), as well as insight into aspects of fundamental physics. Source specific information is, for example, the bulk Lorentz boost factor in a jet model [26] or the optical properties in the source volume [27]. Direct measurement of the bulk Lorentz boost factor (Γ) in a GRB jet remains elusive. Recently reported observations of a spectral cutoff in GRB 090926, however, can be interpreted as a measurement of Γ [28]. For other GRBs only a lower limit is available, e.g. for GRB 090510 $\Gamma \gtrsim 1000$ [18]. During the propagation of gamma rays through the ISM, an attenuation due to interactions with the extra-galactic background light (EBL) is expected [29]. Consequently, the spectral energy cutoff can be a probe for the EBL density. Measurements deliver a relatively high cutoff energy compared to current EBL model predictions [30]. This can be an indicator for physics beyond the standard model [31]. The broad energy range in GRB spectra and the prompt emission, especially in short GRBs, allow for the measurement of bulk Lorentz invariance violation [32, 33].

Because of the important information high-energy gamma rays are able to provide, many instruments for their detection have been installed. Currently three major classes of high-energy detectors exist: Satellite detectors (e.g. [35, 36, 37, 38, 39]), Imaging Atmospheric Cherenkov Telescopes (IACTs) [40] and Extensive Air Shower (EAS) particle detector arrays [41]. Satellites can observe very wide fields of view (e.g. 2.4 sr or 19% of 4π sr for Fermi LAT) and have close to a 100% operational duty cycle. On the other hand, the limited physical size of satellites prevents them from obtaining enough statistics to reach energies greater than tens of GeV. Operating above ≈ 50 GeV IACTs have superb sensitivity and angular and energy resolution. However, IACTs can observe GRBs only in good weather and on moonless nights ($\approx 10\%$ duty cycle for GRBs), and their field of view is restricted to 5 degrees in diameter or less. Therefore the crucial prompt observations may not be possible even with IACTs that have been designed for fast slewing (~ 1 min). EAS detector arrays, such as HAWC, benefit from a very large field of view (≈ 2 sr or 16% of 4π sr) and near 100% duty cycle that will allow for observations in the prompt phase. They are also sensitive to energies beyond those covered by satellites. EAS observatories, in particular HAWC, are thus useful high-energy GRB detectors that complement the observations by satellites such as Fermi. In this paper we will present the sensitivity and capabilities of two methods of detection of GRBs by HAWC and show the observatory's ability to measure possible high-energy emission from GRBs.

2. HAWC

The High Altitude Water Cherenkov (HAWC) observatory is a very high-energy (VHE) gamma-ray detector currently under construction near the peak of Volcán Sierra Negra, Mexico. HAWC is located at 4100 m of altitude, N $18^\circ 59' 48''$, W $97^\circ 18' 34''$. When completed in 2014, HAWC will consist of 300 steel tanks of 7.3 m diameter and 4.5 m deep, covering an instrumented area of about 22,000 m² (the actual tank coverage is 12,550 m²). Each tank will hold a bladder filled with purified water and will contain three 20 cm photomultiplier tubes (PMTs). The PMTs are placed near the bottom of the tank looking up in order to measure prompt Cherenkov light. The inner walls of the bladders are dark to reduce reflections of light. An additional 25 cm, high quantum efficiency PMT will be added to the center of each tank. However, results presented here correspond to simulations of three 20 cm PMTs per tank. The additional PMT will extend HAWC's low energy threshold, improving upon what is presented here. A test array of seven tanks, called VAMOS (Verification And Measuring of Observatory System), has already been built on site. Six of the tanks have been filled with water and instrumented with 4 to 7 PMTs per tank. Engineering data has been collected with 6 tanks. Continuous operation of VAMOS started in Sept 29, 2011. Operation of the first 30

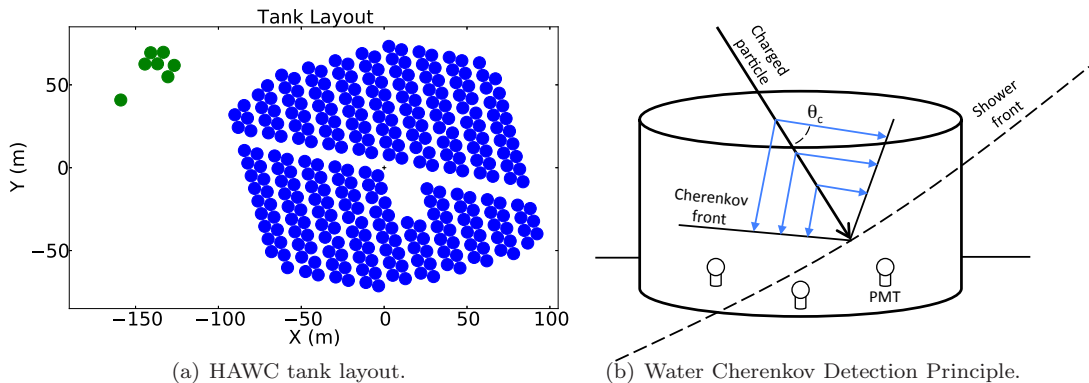


Figure 1: **HAWC layout and operation principle.** The left panel shows the relative position of HAWC tanks. The seven tanks at the top left correspond to VAMOS. The electronics counting house will be at the empty region in the center of the array. The right panel shows the principle of Water Cherenkov Detection. Particles, part of an air shower, arrive at the ground in a shower front. Relativistic charged particles produce Cherenkov radiation as they travel in the water tanks. Cherenkov radiation is emitted at a precise angle θ_c with respect to the particle trajectory. Cherenkov radiation is detected by photomultiplier tubes at the bottom of the tank.

HAWC tanks is expected to start in 2012. A layout of HAWC and VAMOS as well as a description of the water Cherenkov detection method can be seen in figure 1.

HAWC observes gamma rays by detecting, at ground level, the particles that compose an extensive air shower. Charged particles moving through water in the tanks generate Cherenkov light that is captured by the PMTs. Energetic photons traveling through the water in the tanks will typically Compton scatter or produce an electron-positron pair, resulting in Cherenkov light. This latter fact is an advantage of the water Cherenkov method because a large fraction of the electromagnetic component of an air shower at ground level are photons [41].

HAWC improves the sensitivity for a Crab-like point spectrum by a factor of 15 in comparison to its predecessor, Milagro [42] while also extending the reach in the low energy region. The trigger in Milagro used the upper pond layer of 4,000 m², while HAWC uses its entire instrumented area of 22,000 m². For the purposes of discriminating gamma rays from hadrons, Milagro used its deep pond layer of 2,000 m², while HAWC can use its entire instrumented area of 22,000 m². Discrimination of gamma rays and hadrons is also better in HAWC with respect to Milagro because detection elements are optically isolated (tanks vs. single pond). Milagro was complemented by a sparse outrigger array that extended to about 40,000 m² to improve reconstruction capabilities. This is not as necessary in HAWC, as the array is already big enough to provide excellent reconstruction. Finally the higher altitude of HAWC (4100 m vs 2630 m) implies that the detector is closer to the air shower maximum and for a given species of primary, more particles are available at ground level. This is particularly important for the low-energy gamma rays relevant for GRB observations. HAWC will also be able to send quasi-real time alerts (e.g. via the GRB Coordinate Network, or GCN [43]) that can trigger multi-wavelength campaigns. The VERITAS IACT is geographically located close to HAWC, and alerts issued by HAWC may be followed by VERITAS.

HAWC data will be collected by two data acquisition systems (DAQs). The main DAQ will measure the arrival time and time over threshold (TOT) of PMT pulses, hence providing information for the reconstruction of the shower core, direction and lateral distribution, which in turn helps to determine the species of primary particle and its energy. A secondary DAQ, the scaler system, operates in a PMT pulse counting mode [44] and is sensitive to gamma ray and cosmic ray (i.e. due to Solar activity) transient events that produce a sudden increase or decrease in the counting rates with respect to those produced by atmospheric showers and noise.

3. The main DAQ

HAWC's primary DAQ system will record individual events caused by air showers large enough to simultaneously illuminate a significant fraction of the HAWC array. In the simplest approach, depending on the number of hit PMTs during a given time window (trigger condition), a trigger will be issued and sent to time to digital converters (TDCs). The TDCs will store the measured times of the PMT hits closest to the trigger time. The data of each issued trigger are called an event. For the operation of HAWC we plan to use CAEN VX1190 VME TDCs. The final triggering configuration of HAWC is still not defined. As will be shown below, small events contribute significantly to the sensitivity to GRBs.

The event data recorded by the main DAQ system will consist of the leading and trailing edges of discriminated PMT pulses. The Milagro PMTs and front-end boards are being reused in HAWC. The TDCs will measure a pulse's leading and trailing edge at two discriminator settings ($\approx 1/4$ and ≈ 5 photoelectrons). These measurements provide accurate shape to the pulse widths, or TOTs, which can be used to measure the pulse charge over a large dynamic range. The leading and trailing edges will be recorded for two different discriminator thresholds with ≈ 0.5 ns accuracy. Simulations show that an accuracy of 1 ns or better is needed to achieve the best possible angular resolution. Individual events will be time stamped with a GPS clock, with at least 5μ s accuracy. This time stamping will allow HAWC to produce a lightcurve and measure the variability time for GRBs at very high energies. Data collected by the main DAQ will be passed to an online processing computer farm. The location of the air shower core on the ground can be estimated from the spatial distribution of PMT charges and the direction calculated based on the times of the PMT hits produced as the shower front sweeps across the array. The energy of the shower can be estimated from number of PMTs hit, and hadron-induced and photon-induced air showers can be distinguished from each other on a statistical basis by searching for isolated high-amplitude pulses 40 m or more away from the shower core, indicative of muons in hadronic showers. A system to send quasi real time alerts in response to main DAQ gamma-ray transients, e.g. GCN notices, is part of the planned operations of HAWC.

In HAWC, sources of PMT noise are uncorrelated hits from ambient radioactivity in the water and in materials composing PMTs and tanks as well as dark noise from the PMTs. Correlated sources of noise in PMTs, causing several PMTs to fire simultaneously, are secondary gamma rays, electrons and muons from low-energy hadronic cosmic ray showers. First measurements indicate that the total noise hit rate in each PMT is ≈ 20 kHz. The predicted trigger rate is around 5 – 20 kHz, mainly limited by the bandwidth of the TDCs. Examples used in this paper are ≈ 5 and ≈ 17 kHz. We envision a DAQ system with a deadtime of 1% or less.

3.1. The trigger system

In the current design, the trigger system is a distinct piece of hardware that builds a trigger condition based on the number of signals arriving from the front-end boards. This is referred to as a Simple Multiplicity Trigger (SMT). If a trigger condition is satisfied, the trigger signals the TDC to store the data of the PMT hits around the trigger time in a predefined window. An alternative solution is also being investigated that combines a high-throughput TDC readout with a software trigger.

The vast majority of triggers will be produced by hadronic cosmic ray air showers that dominate photon triggers by several orders of magnitude. When a trigger is issued, the data from all PMTs in the array over a time span of 1-2 μ s will be recorded. The data will be processed online by a dedicated computing farm, which includes shower reconstruction algorithms and discrimination of gamma rays from hadrons.

In order to suppress the PMT noise while keeping a high efficiency for shower detection, the DAQ can operate under a set of simple multiplicity triggers with different thresholds. The SMT has two parameters: a minimum number of PMTs above threshold ($nHit$) and a coincidence window (Δt_{trig}). For vertical showers, the particles arrive at HAWC almost simultaneously, while for inclined events they are spread out in time. Hence small values of Δt_{trig} guarantee a high efficiency for vertical showers, while longer windows are required for high efficiency at large angles. Integrating over all angles, air shower particles arrive at HAWC in a time window of 600 ns or less. In this paper we investigate the effect of the two triggers mentioned above on the sensitivity to GRBs. A choice of $nHit = 70$ and $\Delta t_{trig} = 190$ ns leads to ≈ 5 kHz trigger rate. For $nHit = 30$, $\Delta t_{trig} = 190$ ns, the rate will be ≈ 17 kHz.

3.2. The main DAQ simulation and expected performance of the detector

The software employed by Milagro has been modified to simulate HAWC. Galactic cosmic rays are simulated with CORSIKA 6.9 [45] for multiple species with an E^{-2} spectrum: protons, He, C, O, Ne, Mg, Si and Fe. The galactic cosmic ray spectrum is reweighted to match measurements by ATIC [46]. Gamma-ray showers are also simulated using this machinery and reweighted for various source spectra, including power-law spectra as appropriate to describe the high-energy emission of GRBs. The detector response model developed for Milagro and modified for HAWC is used at an altitude of 4100m using a GEANT-4 based code [47]. The simulation used for the main DAQ injects uncorrelated random noise (Poissonian noise) at a rate of 20 kHz per PMT.

The signal rate S is given by

$$S(\theta) = \int dE \frac{dN}{dE} A_{eff}^{trig}(E, \theta), \quad (1)$$

where dN/dE is the photon spectrum and A_{eff}^{trig} is the detector effective area. A_{eff}^{trig} depends on several variables; here only energy E and zenith angle θ are treated.

The effective area of HAWC for gamma rays as a function of trigger level is shown in Fig. 2. Although attenuation of VHE gamma rays via pair production on extragalactic background light (EBL) will limit the energies of gamma rays from GRBs to be below 50-300 GeV (depending on redshift) [29], HAWC retains square meters to tens of square meters of effective area at these energies, values higher than Fermi LAT's 0.8m^2 .

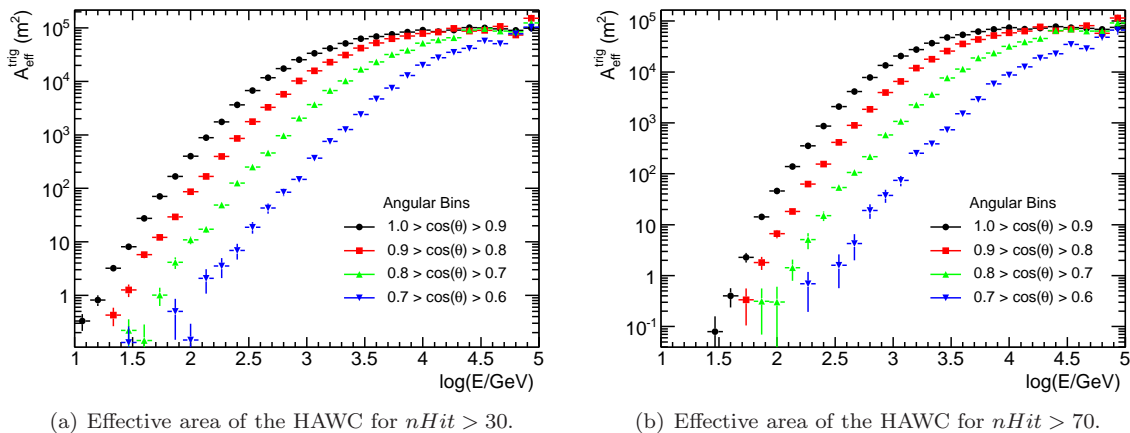


Figure 2: **Effective area of HAWC using the main DAQ system.** Both panels show the effective area A_{eff}^{trig} of HAWC in the triggered mode as a function of γ -ray energy for 4 ranges of zenith angle. A trigger rate of $\approx 17\text{kHz}$ ($nHit > 30$) is assumed in the left panel. A trigger rate of $\approx 5\text{kHz}$ ($nHit > 70$) is assumed in the right panel. Showers reconstructed with $> 1.1^\circ$ error are excluded for the left panel and $> 0.8^\circ$ for the right panel. No gamma-hadron separation cut is applied. For the energies relevant to GRB searches, i.e. below $\approx 300\text{ GeV}$, applying a gamma-hadron separation results in a global reduction of the effective area by a factor of 0.85 (left) and 0.75 (right).

3.3. Sensitivity of the triggered system to GRBs

The sensitivity of HAWC to GRBs depends on a number of factors, including the GRB emission time scale, emission spectrum, elevation and redshift, as well as on the trigger, reconstruction and background rejection capabilities of the experiment. To calculate HAWC's sensitivity, we simulate a gamma ray spectrum according to the power-law $dN/dE \propto E^{-2}$ with an arbitrary reference flux normalization. This injection spectrum can be weighted for any other spectral shapes. In those instances in which we take into account attenuation of VHE gamma rays due to interaction with extragalactic background light, the Gilmore et al. model [29] is used.

After reconstructing the shower core and direction, a hadronic background rejection cut is applied. The background rejection method is based on a quantity called ‘compactness’, defined here as the ratio of the number of PMTs hit in the event to the largest charge on a single PMT hit at a distance of at least 40 m from the reconstructed shower core [48]. Hadronic air showers are both clumpy and muon-rich, and thus tend to exhibit large-amplitude hits at significant distances from the shower axis. On the other hand gamma-ray air showers are muon-poor and hence exhibit a more uniform charge distribution that decreases with distance from the shower core. After applying the gamma-hadron separation cut the gamma ray efficiency is reduced by $\approx 25\%$ for $nHit > 70$ and $\approx 15\%$ for $nHit > 30$. After applying the gamma-hadron separation cut, the background is reduced by $\approx 90\%$ for $nHit > 70$ and $\approx 70\%$ for $nHit > 30$. A cut is also applied to the angular distance between the reconstructed shower direction and position of the source. This implies that the GRB position is known from other observations. The time and duration of the burst are also assumed known, which allows one to efficiently reject the background by defining a restrictive time window.

After all the cuts are applied, the rate of background events remaining is used to determine the minimum number of gamma rays detectable at 5σ significance. Due to the paucity of the number of events involved, the 5σ level is defined using the cumulative Poisson distribution function. The 5σ discovery potential is defined as the flux level which leads to a 50% probability of detecting a 5σ excess. Using this definition implies that for very short bursts ($T \ll 1$ s) the sensitivity scales as $1/T$, while for very long bursts ($T > 3 \times 10^2$ s) the sensitivity scales as $1/\sqrt{T}$. Both the angular distance cut and the hadron rejection cut are optimized to maximize the discovery potential.

Figure 3 displays HAWC’s sensitivity as a function of zenith angle for a 20 s GRB with an E^{-2} spectrum at a redshift of $z = 0.5$ for two different trigger thresholds. As can be seen, the low trigger threshold greatly aids in the detection of GRBs. The background rate within the angle distance cut circle can be parametrized as $R = a \exp(bx + cx^2)$, where $x = \cos\theta$, and θ is the zenith angle. After applying the gamma-hadron separation optimized for GRB search, we find that for $nHit > 70$ ($nHit > 30$), the values of the constants are $a = 0.42$ Hz ($a = 8$ Hz), $b = 7.0$ ($b = 6.6$) and $c = -12.9$ ($c = -8.6$).

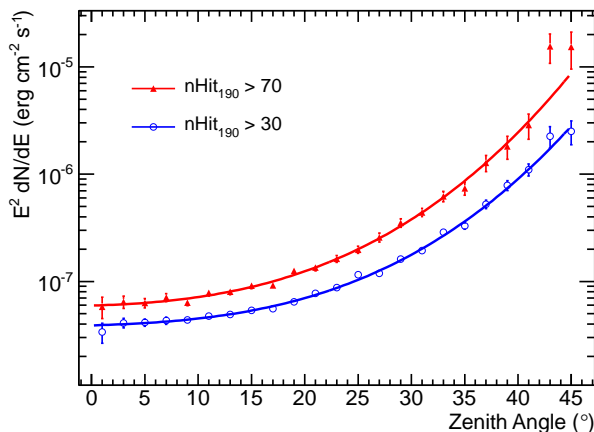


Figure 3: **Sensitivity of HAWC using the main DAQ as a function of zenith angle.** The sensitivity is defined as the flux detectable at 5σ significance with 50% probability. Results are given for the baseline trigger ($nHit > 70$) and a reduced threshold trigger ($nHit > 30$) for a range of zenith angles of an astrophysical source. The simulated burst has a duration of 20 s, a spectral index of -2 and a redshift of 0.5. EBL attenuation is modeled following Gilmore et al. [29].

Figure 4 illustrates the effects of different GRB emission spectra on the expected sensitivity of HAWC using the main DAQ. The two panels of Fig. 4 show the sensitivity curves for two different trigger thresholds assuming that the burst occurs at a zenith angle of 20° and lasts 1 second. We consider a range of spectral indices for spectra of the type $dN/dE \propto E^\gamma$ with various high-energy cutoffs. The effect of EBL is not directly considered because it can be simplistically simulated as a sharp cutoff. As an example, for a redshift of $z = 1$, Gilmore et al. [29] predict a cutoff at about 125 GeV. This choice of spectra is motivated by Fermi LAT observation of GRBs at high-energy [17, 18]. Data for GRBs 090510 and 090902b, extracted

from [18] and [17], are shown for comparison. The reported fluxes of those bursts were scaled by $T^{0.7}$, where T is 0.5 and 30 (seconds) for GRB 090510 and GRB 090902b respectively, to account for the dependence of HAWC’s sensitivity on burst duration as explained previously. HAWC will be able to detect bursts such as GRB 090510 or GRB 090902b with high significance if the high-energy cutoff is above ≈ 100 GeV. In the configuration with the low trigger threshold ($nHit > 30$) cutoff values down to ≈ 60 GeV would be reachable.

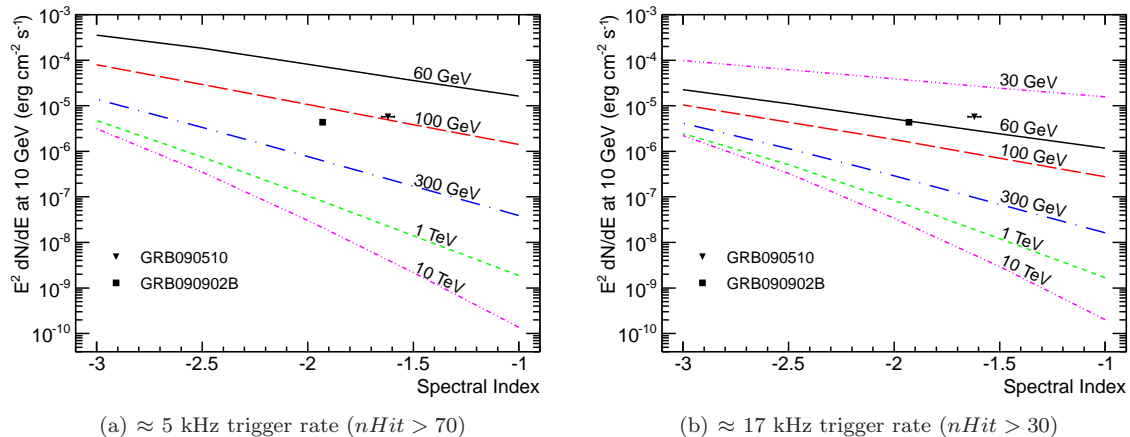


Figure 4: **Sensitivity using the main DAQ as a function of spectral index for two different trigger thresholds.** The 5σ discovery potential is shown as a function of spectral index for various values of a sharp high-energy spectral cutoff. The left plot is for the baseline trigger ($nHit > 70$). The right plot is for an alternative low threshold trigger ($nHit > 30$). The duration of the burst is fixed to 1 s and the zenith angle is fixed to 20° . Data from 2 different GRBs are corrected for duration and inserted for comparison [18, 17].

The present estimates of HAWC sensitivity are based on a simple event counting approach that does not distinguish between low and high energy events. This is equivalent to a binned analysis with a single energy bin. This approach is valid for short transients because of the relatively small number of background events in the search time window. However, for long transients the background contamination becomes important. This is especially true at low energy, where both the gamma-hadron separation and angular reconstruction performance degrade. The resulting energy dependence of the signal-to-noise ratio can be accounted for by defining several energy bins or via an unbinned (likelihood-based) analysis. This should improve the sensitivity upon the baseline values presented here.

The above studies required prior information on a GRB. A simple way to estimate the sensitivity in the case of no prior knowledge of a GRB is to divide the sky and discretize time into bins and apply the technique described above to each bin. This leads to a large trial factor which has to be compensated for by requiring more events. The division of a 2 sr field of view into bins of 0.7° radius leads to $\approx 10^4$ bins, or 10^4 trial factor per time bin. Time discretization depends on assumed GRB duration. For example, dividing 1 year of data into 1 s intervals leads to a trial factor of 3×10^7 . So the total trial factor is greater than 3×10^{11} because of oversampling. To make a 5σ level observation the pre-trial factor observations would need to be $\approx 8.5\sigma$ (p-value of 1.8×10^{-18}). This corresponds to a loss in sensitivity of less than a factor of 2. For example, for a 1 second burst 13 events would be needed instead of 7 when an external trigger such as GCN is used.

4. The scaler DAQ

Ground based air shower arrays are sensitive to gamma-ray transients, GRBs in particular, in the GeV-TeV range using the single particle or scaler technique [44]. During regular operations, the counts in HAWC’s PMTs are due to cosmic ray air showers, naturally occurring radioactivity near the PMTs and thermal noise in the PMTs. This system can be used to monitor the health of the detector and to study particle emission by the Sun [49], such as protons, neutrons and ions. By monitoring PMTs at low threshold

(> 1/4 photoelectron), the scaler system is sensitive to gamma-ray transients. While the scaler system is not able to provide directional information, it is complementary to the trigger system and to other detectors, such as Fermi LAT, that are sensitive to gamma-ray transients. For the operation of HAWC we plan to use Struck SiS-3820 VME scalars.

All 900 PMT rates will be monitored in 10 ms windows. This fine time sampling will allow the scaler system to produce a lightcurve and measure the variability of GRBs at very high energies. As described before, each PMT is expected to have a rate of ≈ 20 kHz. A transient flux of gamma rays will result in a detector wide increase of the PMT rate, thus gamma-ray transients are identified on a statistical basis. Low energy gamma rays from GRBs that are not observed by the main DAQ may still be observable by the scaler system. Issuing quasi-real time alerts is not being considered as part of the default operation of HAWC scalars, but we will distribute GCN circulars describing HAWC scaler observations of GRBs as appropriate.

4.1. Signal Simulation for the scaler DAQ

Signal simulation has been performed with the same software as the main DAQ. The energy range for primary showers was set to 0.5 GeV - 10 TeV, because we expect the scalars to have sensitivity to lower energy gamma rays than the main DAQ. Photons of energy as low as a few GeV can have a significant contribution to the scaler signal. The signal rate S in the scaler system is the number of PMT counts expected on excess of the nominal PMT rate. This signal rate S is given by

$$S(\theta) = \int dE \frac{dN}{dE} A_{eff}^{scaler}(E, \theta), \quad (2)$$

where dN/dE is the photon spectrum and A_{eff}^{scaler} is the effective area for the scaler system. Because each atmospheric shower can cause hits in multiple PMTs, the scaler effective area is:

$$A_{eff}^{scaler}(E, \theta) = A_{thrown} N_{PMT} \frac{N_{obs}(E, \theta)}{N_{thrown}(E, \theta)}, \quad (3)$$

where A_{thrown} is the area over which simulated events are thrown, N_{obs} is the number of showers that result in at least one PMT being hit, N_{thrown} is the number of simulated showers and N_{PMT} is the average number of PMTs hit for energy E and zenith θ . Because the scaler DAQ signal is the number of PMT hits and not individual air showers, the value for the effective area is not restricted to the physical detector size. We have used the same simulation as the main DAQ system to calculate the scaler effective area A_{eff}^{scaler} of HAWC. The scaler effective area as a function of energy for various zenith bands is shown in Fig. 5. Besides simulating HAWC with 300 tanks and 3 PMTs per tank as described in Sec. 2, we have also simulated intermediate steps in the construction of HAWC, such as HAWC with 30 tanks and with 100 tanks. We also investigated tanks that are instrumented with as many as 7 PMTs per tank. In this PMT/tank range, the scaler effective area scales as N_{PMT} , the total number of PMTs and/or tanks in the detector.

4.2. Background simulation for the scaler DAQ

We expect the total (> 1/4 photoelectron) rate in the detector to be $B = 18$ MHz (20 kHz \times 900). Even if the number of air showers in given time intervals can be considered to follow a Poissonian distribution, the distribution of the total noise rate B is not Poissonian. This is because some of the sources of noise are correlated. Sources that produce two or more PMT signals in the detector result in a distribution that is wider than a Poissonian because of *double counting* in the measured average. In order, the most important sources of correlation are: (a) air showers resulting in more than one PMT registering a signal, (b) PMT afterpulses and (c) Michel electrons due to muons that stop inside HAWC tanks. The correlations result in a distribution that is wider than a Poissonian. The Fano factor F [50] describes how much wider the real distribution is with respect to a Poissonian with the same mean value but no correlation: $\sigma_B^2 = F B$. Given

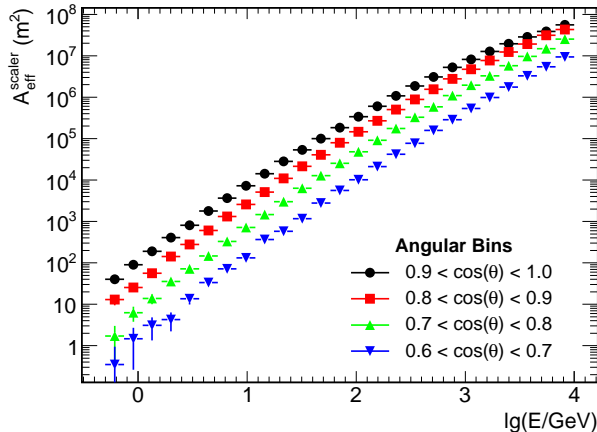


Figure 5: **Effective area of the HAWC scaler system.** The scaler effective area A_{eff}^{scaler} is shown for 4 zenith angle bins.

a signal rate S , background rate B and Fano factor F , then the significance of a given observation is:

$$\begin{aligned} \text{Sigf} &= \frac{S \Delta T}{\sqrt{F \Delta T B}} \\ &= \sqrt{\frac{\Delta T}{F N_{PMT} R_{PMT}}} \int_{E_{min}}^{E_{max}} dE \frac{dN}{dE} A_{eff}^{scaler}(\theta), \end{aligned} \quad (4)$$

where N_{PMT} is the number of PMTs in the detector, R_{PMT} is the average PMT rate, ΔT is the observation window and θ is the zenith of the GRB being studied. Note that since the background rate B scales as N_{PMT} , and since the scaler effective area also scales as N_{PMT} , then Eq. 4 implies that the significance of observations scales as $\sqrt{N_{PMT}}$. However the dependence of the Fano factor on N_{PMT} has not yet been studied.

During the operation of HAWC, the width of the noise distribution, and hence the Fano factor, will be measured experimentally. In the mean time, we have developed a dedicated background simulation to describe the PMT noise rate and calculate the Fano factor. The objective of the simulation is not to produce a series of distinct *events* as customary in particle physics simulation, but to produce a PMT *hit stream* as measured by the scalars.

The simulation begins similarly to that of the main DAQ with a set of cosmic ray events simulated with CORSIKA and a GEANT4-based detector simulation. We assume an $E^{-2.7}$ power-law distribution for the primary cosmic rays and normalize the rate with the ATIC measurements at high energies (≈ 100 GeV) [46]. Below 10 GeV the cosmic ray spectrum is affected by the solar modulation and the Earth's magnetic field. Because the value of the Fano factor is almost independent of the shape of the spectrum at low energies (Fig. 6(a)) a detailed description of the spectrum is not critical. We simulate the geomagnetic cutoff (≈ 8 GeV at the HAWC site) as a sharp cutoff, but again, this choice is not critical. The result of this simulation is a series of air showers each including a list of ideal photoelectrons (i.e. not including the effects of electronics). The time of each air shower is assigned randomly as expected from the assumed spectrum and the list of photoelectrons is time sorted, i.e. a photoelectron stream is produced.

Uncorrelated Gaussian noise is added to the photoelectron stream. This noise is expected to originate from thermal noise, radioactive decays near or in the PMTs, etc. We considered rates in the range of 5 kHz to 30 kHz. We assume a default value of 7.5 kHz. If a higher rate is assumed the Fano factor decreases, leading to almost the same sensitivity. Therefore, for the ranges considered the choice of uncorrelated PMT noise is not critical.

The photoelectron stream is then further modified by adding PMT afterpulses. The afterpulsing characteristics of HAWC PMTs are not known yet, so we have used data for AMANDA (8 inch) and IceCube

(10 inch) PMTs as a reference. Each photoelectron is assigned a 6% probability of producing an afterpulse per photoelectron.

The final step is a simplistic electronics simulation. The HAWC front-end boards will enforce a minimum width for discriminated PMT pulses of 20 ns (as a reference, the average 1 photoelectron pulse at low threshold will be ≈ 150 ns). We merge all photoelectrons that are in coincidence in this time window and call the resulting list a PMT hit stream. This electronics simulation is conservative and will result in a larger Fano factor than a more detailed simulation. Thus our crude electronics description does not result in overestimating the scaler sensitivity.

The final hit stream is then binned into the scaler time windows (Fig. 6(b)). Using the default parameters we obtain a Fano factor of 17.4, which reduces the sensitivity of HAWC scalars by a factor of 4.2 with respect to assuming Poissonian PMT noise.

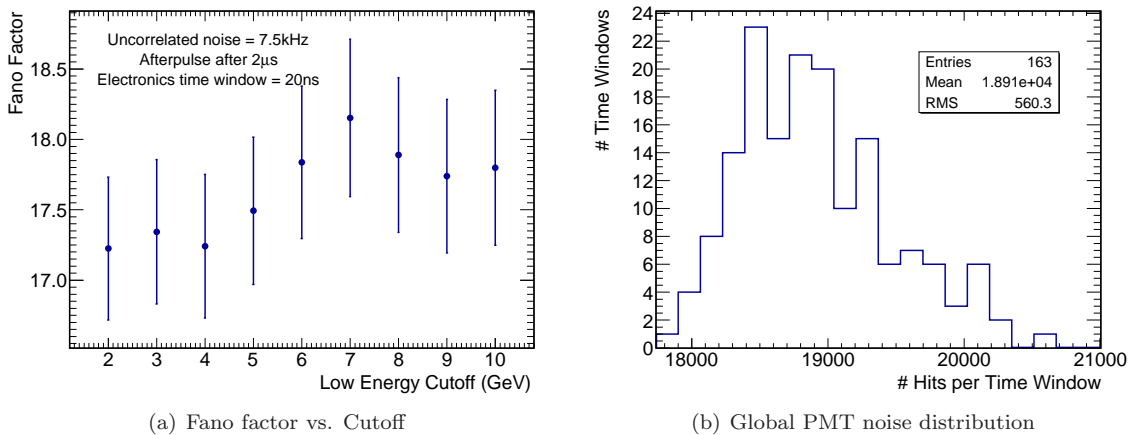


Figure 6: **Simulation of the noise rate of the HAWC scaler system.**

4.3. Sensitivity of the scaler system to GRBs

We have used various spectra of the type $dN/dE \propto E^\gamma$ with sharp high-energy cutoffs to determine the sensitivity of the scaler system to gamma-ray transients. A range of spectral indices γ between -3 and -1 and a range of cutoffs between 10 GeV and 10 TeV were tested, similar to those examined by the main DAQ. Again, effects of the EBL are ignored.

An interesting question is whether HAWC scalars are able to observe the same GRBs that have been seen by Fermi LAT. Figure 7 shows HAWC's sensitivity, calculated with equation 4 compared to GRBs that have been detected by Fermi LAT. We conclude that the most promising cases for detection are GRBs that have a non-Band hard power-law component such as GRB 090510 and 090902b. Fermi LAT observations of these two GRBs were made up to 30 GeV without any indication of a cutoff. Therefore HAWC scalars would observe GRBs similar to 090510 if they were to happen again within a zenith range of $0 - 26^\circ$ (equivalently $0.9 < \cos \theta < 1.0$ or 0.065 sr). If high-energy emission from GRBs extends beyond 30 GeV, then HAWC scaler observations become even more significant while Fermi LAT struggles due to limited physical size. If high-energy emission extends up to 100 GeV, the HAWC scalars can make observations in a field of view of 0.125 sr ($0 - 37^\circ$ zenith range).

Also interesting is to compare the sensitivity of HAWC to other detectors that use the single particle technique. Because of size, high altitude, better design (optically isolated water Cherenkov detectors, as opposed to single ponds, scintillators or resistive plate chambers), HAWC will be at least one order of magnitude more sensitive than Milagro [52], Pierre Auger [53], LAGO [54], ARGO [55], etc. Our simulations show that even VAMOS using scalars is slightly more sensitive than Milagro. Note that even though LAGO is at a significantly higher altitude and has a similar design to HAWC, it is significantly smaller.

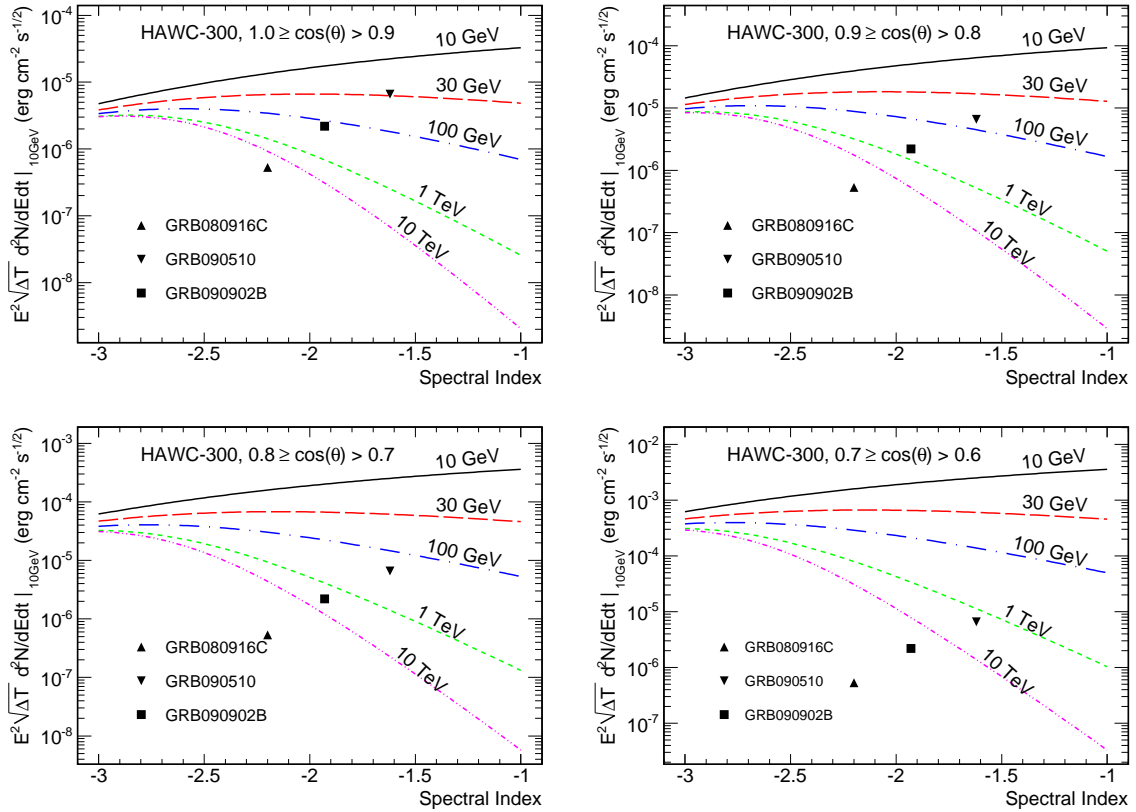


Figure 7: **Sensitivity of the scaler system to GRBs.** Necessary flux at 10 GeV multiplied by the square root of the GRB duration to produce a 5σ signal in the HAWC scaler system. The scaler sensitivity is proportional to $\sqrt{\Delta T}$. We assume that the GRB spectrum includes a power-law component with index γ and a hard cutoff in addition to the standard Band function. At the energies to which HAWC is sensitive, only the power-law component is relevant. The plots for five different cutoff energies are shown in each picture. Each picture refers to a specific zenith angle bin. Data from 3 different GRBs are inserted for comparison [51, 18, 17].

5. Joint sensitivity of main DAQ and scaler DAQ to GRBs

At a basic level the information provided by both the main DAQ and scaler system will be a measure of the strength of the signal, which corresponds to the number of events for the main DAQ and the significance of the observation for the scaler DAQ. The main DAQ allows for event by event energy reconstruction. Above ≈ 1 TeV the energy can be reconstructed from the data taken with the triggered DAQ system. However at energies below ≈ 1 TeV, the showers detected by HAWC are those in which the first interaction happens lower than average in the atmosphere. At first glance, the difficulty of HAWC to reconstruct energy in the range relevant to GRBs, may seem as a drawback. However observations of GRBs by HAWC can be combined with other detectors that have different energy response leading to constrains in the spectrum. Furthermore, the energy responses of scalers and the main DAQ are different. Their combined observations (or lack of) can be used to constrain the very high energy spectrum.

The sensitivity of the scaler and main DAQs to GRBs are complementary: the scaler DAQ covers a lower energy range and is able to provide information on sudden increased rates whereas the main DAQ can reconstruct the energy and direction of events at somewhat higher energy. Both systems will help provide information on the spectra of GRBs. Figure 8 shows the minimum flux required to make a 5σ detection of a transient source with a zenith angle of 20° and a duration between 10^{-2} and 5×10^3 s for both scalers and the main DAQ. The trigger used by the main DAQ is a simple multiplicity trigger of 70 PMTs hit. Also

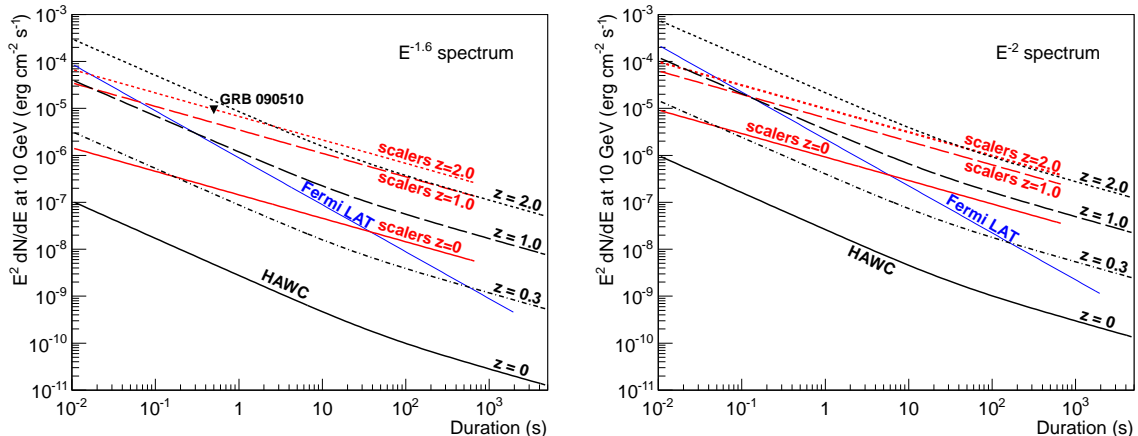


Figure 8: **Sensitivity of HAWC using the main DAQ and scalars as a function of burst duration.** The main DAQ uses a simple multiplicity trigger of 70 PMTs or more. The source position is set at a zenith angle of 20° . The source spectrum is $E^{-1.6}$ and $E^{-2.0}$ for the left and right plots respectively. The Gilmore model of gamma ray attenuation by EBL [29] is used to obtain the sensitivity curves for different redshifts. The lines for the scalars reflect the 5σ discovery level. For the main DAQ the lines define the 5σ discovery potential. Also shown is the flux necessary for the observation of 1 photon above 10 GeV by Fermi LAT. A marker is inserted in the left plot for GRB 090510 [18].

shown is the sensitivity of Fermi LAT assuming that at least one > 10 GeV photon is detected. The figure includes the effects of EBL as modeled by Gilmore et al. [29] at various values of redshift. Precisely because the energy response of the scalars and main DAQ are different, the effects of EBL are different for both techniques. The effects of a softer spectrum are less pronounced on the scaler system. For all durations the sensitivity of scalars is proportional to $1/\sqrt{\Delta T}$ as described in section 4.3. For the main DAQ, the time dependence of flux sensitivity is more complicated. At long durations, the background is large enough so that the sensitivity scales as $1/\sqrt{\Delta T}$. At short durations the background is very small and the sensitivity of the main DAQ is roughly proportional to $1/\Delta T$.

We assume that the high-energy spectrum of a GRB may be described by three parameters: the flux normalization at, in our case, 10 GeV, the spectral index and a high-energy cutoff. The high-energy cutoff is a quantity that is particularly interesting to measure as it provides information about the bulk Lorentz boost factor of the GRB jet, probes the EBL or provides information about the highest energy to which GRBs accelerate particles. Depending on whether various satellites or ground based instruments study a given GRB, then various parameters of the high-energy spectrum can be constrained or measured.

As an example of how external information and a joint scaler-main DAQ analysis could be performed we use a sample GRB. This GRB is assumed to have similar, but not identical, characteristics to GRB 090510. We use

$$\frac{dN}{dE} = C \left(\frac{E}{1 \text{ GeV}} \right)^\gamma \quad (5)$$

and assume dN/dE at 10 GeV to be $0.58 \text{ GeV}^{-1} \text{ m}^{-2} \text{ s}^{-1}$ (or $E^2 dN/dE = 9.32 \times 10^{-6} \text{ erg cm}^{-2} \text{ s}^{-1}$), a high energy spectral index of -1.6 and a Heaviside high-energy cutoff at 150 GeV. We set the zenith angle to 20° . EBL absorption is ignored because the objective of this example is to illustrate how both systems in combination can measure a spectral cutoff. Using the simulations described above, we obtain 17 expected events for the sample GRB seen by the main DAQ and $\approx 200,000$ PMT hits over typical background for the scaler system, leading to an 11σ significance by the scaler system for this reference GRB.

We now assume that the main (scaler) DAQ system delivered the number of events (significance) computed above and test the ability of a combined analysis to constrain the spectral parameters. In order to find the region of the parameter space consistent with the measurements, the simulation described above is repeated for various values of a hypothetical Heaviside high-energy cutoff and spectral index. For each point on the spectral index – cutoff plane, the computed number of events (significance) is used to find the

value of dN/dE at 10 GeV which corresponds to the measured number of events (significance). The values delivered by the main DAQ and scalers are then compared to find the region where they are consistent. The allowed region, assuming a 25% error bar between the two measurements, is shown in Fig. 9. As can be seen, the combined analysis yields meaningful constraints on the GRB spectrum. The allowed region could be further narrowed down by including data from other experiments (e.g. Fermi) and theoretical constraints. It should be noted that the values of dN/dE at 10 GeV, obtained with scalers, vary by $\approx \pm 40\%$ throughout the allowed region. Within this error bar, the measurement of the flux normalization is independent of the spectral parameters measurement. A similar technique was employed in [20] to constrain spectral parameters of GRB 970417a.

In this example we have taken into account the statistical uncertainties of the signal expectation in the main DAQ system, shown as a band in Fig. 9. However the statistical uncertainty in the scaler system is extremely small. Therefore the uncertainty of the measurement by the scalers is dominated by still unknown systematic uncertainties. The variation of PMT noise rates due to upper atmospheric conditions (which in turn affect air shower development), local weather and instrumental effects are expected to be the main sources of systematic uncertainties in the scaler system.

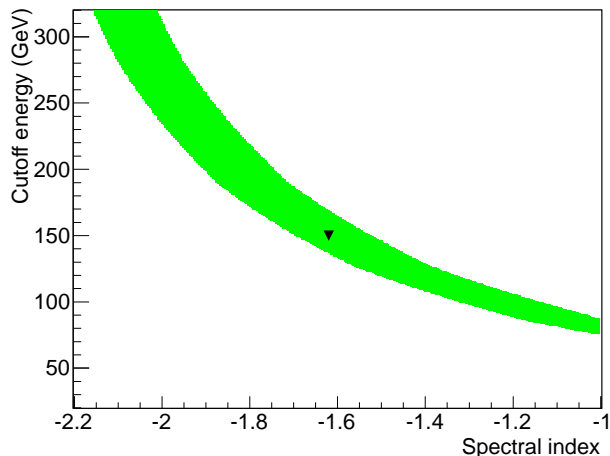


Figure 9: **A simulation of a measurement constraining the spectral index and cutoff of a GRB.** The simulation combines the information from the main DAQ (with trigger threshold $nHit > 70$) and the scalers. The simulated GRB spectrum has a spectral index of -1.62 and a Heaviside cutoff at 150 GeV (shown by black triangle). The flux normalization, chosen to match GRB 090510, was used to set a significance level in both DAQ systems. The green band shows the region where the flux values derived from the observations by the two systems agree within $\pm 25\%$. Systematic errors are not included.

This example demonstrates that through the operation of the scaler system and the main DAQ, HAWC will be able to extend the sensitivity to high-energy emission by GRBs to energies currently inaccessible to Fermi LAT, while performing prompt observations. In particular it will be able to make measurements of a high-energy spectral cutoff. Future studies with real GRBs will use more detailed information and uncertainties provided by external sources such as sky localization, redshift, spectrum, etc.

6. Scientific prospect and conclusions

HAWC, a ground based EAS detector, will have the capability of detecting GRBs at high energies. The simulations presented in this paper show that HAWC will be able to detect GRBs with characteristics similar to those of some of the brightest GRBs seen by Fermi LAT. In particular we have shown that if bursts such as GRB 090510 were to repeat with a zenith angle of 26° or less they would be detected with 5σ or greater significance. HAWC will be particularly useful for GRBs with hard non-Band power-law high-energy spectral components. Two methods for detection of GRBs will be used by HAWC. The main DAQ will acquire and reconstruct data on a shower by shower basis. The scaler system will search for a

statistical excess on the combined noise rate of all PMTs. As opposed to Fermi LAT, with a fixed physical size, the effective area of both scalers and main DAQ increases with energy. Thus either of the explained detection methods will expand upon the energy sensitivity of current detectors. Also, because HAWC is a wide field of view detector with near 100% duty cycle, it will be able to make GRB observations in the prompt phase. An example of how to perform a joint study of GRB spectra using both scalers and the main DAQ was shown. HAWC, in unison with satellite or ground based detectors, will be able to measure the high-energy GRB components including a possible high-energy cutoff. Important astrophysical information will be deduced from spectral cutoffs such as the bulk Lorentz boost factor of GRB jets, the effects of the EBL and the maximum energy to which GRBs accelerate particles.

Acknowledgements

This work has been supported by: the National Science Foundation, the US Department of Energy Office of High-Energy Physics, the LDRD program of Los Alamos National Laboratory, Consejo Nacional de Ciencia y Tecnología (grants 55155, 103520, 105033, 105666, 122331 and 132197), Red de Física de Altas Energías, DGAPA-UNAM (grants IN105211, IN112910 and IN121309, IN115409), VIEP-BUAP (grant 161-EXC-2011) and the University of Wisconsin Alumni Research Foundation.

References

- [1] N. Gehrels, E. Ramirez-Ruiz, & D. B. Fox, Gamma-Ray Bursts in the Swift Era, *Ann. Rev. A&A*, 47 (2009) 567-617
- [2] J. L. Racusin et al., Broadband observations of the naked-eye big gamma-ray burst GRB 080319B, *Nature* 455 (2008) 183-188
- [3] M. Ruffert & H. T. Janka, Gamma-ray bursts from accreting black holes in neutron star mergers, *A&A* 344 (1999) 573-606
- [4] S. Rosswog, E. Ramirez-Ruiz, M. B. Davies, High-resolution calculations of merging neutron stars III. Gamma-ray bursts, *MNRAS* 345 (2003) 1077-1090
- [5] T. A. Thompson et al., Magnetar Spin-Down, Hyperenergetic Supernovae, and Gamma-Ray Bursts, *ApJ* 611 (2004) 380
- [6] S. E. Woosley, Gamma-ray bursts from stellar mass accretion disks around black holes, *ApJ* 405 (1993) 273-277
- [7] A. MacFadyen, S. E. Woosley, Collapsars: Gamma-Ray Bursts and Explosions in Failed Supernovae, *ApJ* 524 (1999) 262
- [8] P. Mészáros, Gamma-Ray Bursts: Accumulating Afterglow Implications, Progenitor Clues, and Prospects, *Science* 291 (2001) 79-84
- [9] P. Mészáros, Gamma-ray bursts, *Rept. Prog. Phys.* 69 (2006) 2259
- [10] T. Piran, Gamma-Ray Bursts and the Fireball Model, *Physics Reports* 314 (1999) 575-667
- [11] D. Lazzati et al., Gamma-ray burst jet dynamics and their interaction with the progenitor star, *Phil. Trans. R. Soc. A* 365 (2007) 1141-1149
- [12] N. R. Tanvir et al., A bold gamma-ray burst at a redshift of z approximately 8.2, *Nature* 461 (2009) 1254
- [13] C. Kouveliotou et al., Identification of Two Classes of Gamma-Ray Bursts, *ApJ* 413 (1993) L101
- [14] D. Band et al., BATSE Observations of Gamma-Ray Burst Spectra. I. Spectral Diversity, *ApJ* 413 (1993) 281
- [15] M. González et al., A gamma-ray burst with a high-energy spectral component inconsistent with the synchrotron shock model, *Nature* 424 (2003) 749-751
- [16] C. Wigger, O. Wigger, E. Bellm, W. Hajdas, Observation of an Unexpected Hardening in the Spectrum of GRB 021206, *ApJ* 675 (2008) 553
- [17] A. Abdo et al., Fermi Observations of GRB 090902B: A Distinct Spectral Component in the Prompt and Delayed Emission, *ApJ* 706 (2009) L138
- [18] M. Ackermann et al., Fermi Observations of GRB 090510: A Short Hard Gamma-Ray Burst with an Additional, Hard Power-Law Component from 10 keV to GeV Energies, *ApJ* 716 (2010) 1178-1190
- [19] S. Guiriec, Fermi GBM Observations of Three Intense Short GRBs, 2nd Fermi Symposium. Washington DC, USA (2009)
- [20] R. Atkins et al., The High-Energy Gamma-Ray Fluence and Energy Spectrum of GRB 970417a from Observations with Milagro, *ApJ* 583 (2003) 824-832
- [21] A. Abdo et al., Milagro Constraints on Very High Energy Emission from Short-Duration Gamma-Ray Bursts, *ApJ*, 666 (2007) 361-367
- [22] R. Atkins et al., Constraints on Very High Energy Gamma-Ray Emission from Gamma-Ray Bursts, *ApJ*, 630 (2005) 996-1002
- [23] R. Atkins et al., Limits on Very High Energy Emission from Gamma-Ray Bursts with the Milagro Observatory, *ApJ*, 604 (2004) L25-L28
- [24] S. Razzaque, C. D. Dermer, J. D. Finke, Synchrotron radiation from ultra-high energy protons and the Fermi observations of GRB 080916C, *The Open Astronomy Journal*, 3 (2010) 150-155
- [25] G. Ghirlanda, G. Ghisellini, L. Nava, The onset of the GeV afterglow of GRB 090510, *A&A* 510 (2010) L7-L11
- [26] J. E. Rhoads, How to Tell a Jet from a Balloon: A Proposed Test for Beaming in Gamma-Ray Bursts, *ApJ* 487 (1997) L1
- [27] R. C. Gilmore, E. Ramirez-Ruiz, Local absorption of high-energy emission from gamma-ray bursts, *ApJ* 721 (2010) 709-714

- [28] M. Ackermann et al., Detection of a spectral break in the extra hard component of GRB 090926A, *ApJ* 729 (2011) 114
- [29] R. C. Gilmore, et al., GeV gamma-ray attenuation and the high-redshift UV background, *MNRAS* 399 (2009) 1694-1708
- [30] J. Albert et al., Very-High-Energy gamma rays from a Distant Quasar: How Transparent Is the Universe?, *Science* 320 (2008) 1752
- [31] M. A. Sánchez-Conde, et al., Hints of the existence of axionlike particles from the gamma-ray spectra of cosmological sources, *Phys. Rev. D* 79 (2009) 123511
- [32] M. Biesiada, A. Piorkowska, Lorentz invariance violation-induced time delays in GRBs in different cosmological models , *Class. Quant. Grav.* 26 (2009) 125007
- [33] A. Abdo et al., A limit on the variation of the speed of light arising from quantum gravity effects, *Nature* 462 (2009) 331-334
- [34] D. Q. Lamb, D.E. Reichart, Gamma-Ray Bursts as a Probe of the Very High Redshift Universe , *ApJ* 536 (2000) 1
- [35] N. Gehrels et al., The Compton Gamma Ray Observatory, *ApJS* 92 (1994) 351
- [36] D. J. Thompson et al., The Highest-Energy Photons Seen by the Energetic Gamma Ray Experiment Telescope (EGRET) on the Compton Gamma Ray Observatory, *ApJS* 157 (2005) 324
- [37] W. B. Atwood et al., The Large Area Telescope on the Fermi Gamma-ray Space Telescope Mission , *ApJ* 697 (2009) 1071
- [38] Meegan C. et al., The Fermi Gamma-ray Burst Monitor, *ApJ* 702 (2009) 791-804
- [39] N. Gehrels, The Swift Gamma Ray Burst Mission, *New Astron. Rev.* 48 (2004) 431
- [40] J. Hinton, Ground-based gamma-ray astronomy with Cherenkov telescopes, *New J. Phys.* 11 (2009) 055005
- [41] G. Sinnis, Air shower detectors in gamma-ray astronomy, *New J. Phys.* 11 (2009) 055007
- [42] R. Atkins, TeV Gamma-Ray Survey of the Northern Hemisphere Sky Using the Milagro Observatory, *ApJ* 608 (2004) 680
- [43] S. D. Barthelmy et al. GRB Coordinates Network (GCN): A Status Report, *Proc 4th Huntsville GRB Symposium*, 428 (1999) 99
- [44] S. Vernetto, GRB Coordinates Network (GCN): A Status Report
- [45] J. Knapp, D. Heck, G. Schatz, Comparison of Hadronic Interaction Models Used in Air Shower Simulations and of Their Influence on Shower Development and Observables, *FZKA report* 5828 (1996)
- [46] A. D. Panov et al., Energy Spectra of Abundant Nuclei of Primary Cosmic Rays from the Data of ATIC-2 Experiment: Final Results, *Bull. Russian Acad. Sci., Physics* 73 (2009) 564
- [47] S. Agostinelli et al., Geant4 - A Simulation Toolkit, *NIM A* 506 (2003) 250
- [48] R. Atkins et al., Observation of TeV Gamma Rays from the Crab Nebula with Milagro Using a New Background Rejection Technique, *ApJ* 595 (2003) 803
- [49] A. Falcone et al., Observation of GeV Solar Energetic Particles from the 1997 November 6 Event Using Milagrito, *ApJ* 588 (2003) 557
- [50] U. Fano, Ionization Yield of Radiations. II. The Fluctuations of the Number of Ions, *Phys. Rev.* 72 (1947) 26-29
- [51] M.S. Briggs et al., Fermi Observations of High-Energy Gamma-Ray Emission from GRB 080916C, *Science* 323 (2009) 1688-1693
- [52] T. Aune et al., Search for 1-100 GeV Emission from Gamma-Ray Bursts Using Milagro, *Proc. 31st International Cosmic Ray Conference* 3 (2008) 1139-1142
- [53] X. Bertou et al., Search for Gamma Ray Bursts using the single particle technique at the Pierre Auger Observatory, *Proc. 30th International Cosmic Ray Conference*, 4 (2008) 4 441-444
- [54] D. Allard et al., Use of water-Cherenkov detectors to detect Gamma Ray Bursts at the Large Aperture GRB Observatory (LAGO), *Nuclear Instruments and Methods in Physics A* 595 (2008) 70-72
- [55] A. Budano et al. Search for gamma ray bursts with the ARGO-YBJ detector in scaler mode, *ApJ* 699 (2009) 1281-1287